Hybrid Materials

DOI: 10.1002/anie.200501748

Thermolysis of a Hybrid Organic–Inorganic Supramolecular Coordination Assembly: Templating the Formation of Nanostructured Fibrous Materials and Carbon-Based Microcapsules**

Wolfgang Schmitt, Jonathan P. Hill, Sharali Malik, Cynthia A. Volkert, Izumi Ichinose, Christopher E. Anson, and Annie K. Powell**

Materials of nanosize or bearing nanoscale features represent a significant class of substance that have the potential for advanced applications because of their superior chemical and physical properties.[1] The preparation and characterization of such substances is, therefore, of interest not only from a scientific viewpoint but because of their possible uses in such diverse fields as catalysis[2] and microelectronics.[3] Currently, much attention is focused on inorganic nanotubes, organic polymers, and nanostructured inorganic oxides whose properties endow them with considerable potential.[4]

The structures and properties of nanosized hybrid organic–inorganic materials are influenced by the functionalities present in both the inorganic and organic components,[5] whereas the use of coordination compounds as templates or precursors in decomposition processes is a

[*] Dr. W. Schmitt, Dr. J. P. Hill, Dr. C. E. Anson, Prof. A. K. Powell
Institut für Anorganische Chemie
Universität Karlsruhe
Engesserstrasse Geb. 30.45, 76128 Karlsruhe (Germany)
Fax: (+49) 721-608-8142
E-mail: schmitt.wolfgang@nims.go.jp
powell@chemie.uni-karlsruhe.de

Dr. W. Schmitt, Dr. J. P. Hill
National Institute for Materials Science
International Centre for Young Scientists
Tsukuba, 1-1 Namiki, Ibaraki 305 0044 (Japan)
Fax: (+81) 29-860-4708

Dr. S. Malik
Institut für Nanotechnologie (INT)
Forschungszentrum Karlsruhe
76344 Eggenstein-Leopoldshafen (Germany)

Dr. C. A. Volkert
Institut für Materialienforschung (IMF)
Forschungszentrum Karlsruhe
76344 Eggenstein-Leopoldshafen (Germany)

Dr. I. Ichinose
Advanced Materials Laboratory
National Institute for Materials Science
1-1 Namiki, Tskuba, Ibaraki 305-0044 (Japan)

[**] This work was supported by the DFG "Center for Functional Nanostructures (CFN)" and the Special Coordination Funds for Promoting Science and Technology from MEXT, Japan through ICYS Fellowships (W.S. and J.P.H.).

Supporting information for this article is available on the WWW under http://www.angewandte.org or from the author.

promising strategy for the synthesis of nanocomposites.[6] Supramolecular coordination compounds that contain nanosized features within their structures are ideal precursor candidates for these purposes. One aim of such investigations is to develop an understanding of how the structures of the precursor complexes influence the structure and stoichiometry of the decomposition products. Thermolysis of metal complexes is already widely used for the synthesis of superconducting, nanocrystalline mixed-metal oxides[7] and also for the incorporation of transition-metal ions into porous carriers, such as zeolites or silicates.[8] Hybrid materials themselves can have unique properties, and their synthesis on the atomic-to-mesoscopic scales can have significant impact on diverse fields of technology.[9]

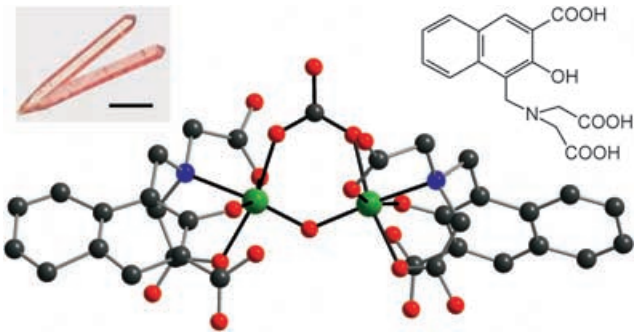

Figure 1. Structure of the dinuclear $[Fe_2(\mu\text{-}O)(\mu\text{-}CO_3)(chnida)_2]^{6-}$ unit contained in **1** (Fe: green, O: red, N: blue, C: gray). Inset: crystals of **1** (left; scale bar: 300 μm) and the organic chnida ligand (right).

Reaction systems that contain large organic hydrophobic ligands and hydrophilic ions favor the formation of cross-linked structures in which supramolecular aggregates are organized within vast areas of different polarities. We have previously described how increased steric hindrance around aromatic cycles (L) influences the topology and dimensionality of coordination chemistry networks based on $\{Fe_2(\mu\text{-}O)(\mu\text{-}CO_3)(L)_2\}$ units,[10,11] thus bringing a new dimension to the now classical isoreticular chemistry concept. Herein, we describe the pyrolysis of an example of one of these compounds. The coordination network used in these investigations, $Na_6[Fe_2(\mu\text{-}O)(\mu\text{-}CO_3)(chnida)_2]\cdot 13.5\,H_2O$ (**1**; chnida = *N*-[(3-carboxy-2-oxy-naphthyl)methylene]iminodiacetato), consists of a simple oxo/carbonato bridged diiron(III) unit coordinated by two chnida ligands. Figure 1 shows the basic diiron unit $[Fe_2(\mu\text{-}O)(\mu\text{-}CO_3)(chnida)_2]^{6-}$ within the structure of complex **1**, together with the chemical structure of the ligand and an optical micrograph of crystals of the complex. Within the dinuclear transition-metal complex, nitrogen and oxygen donors of the iminodiacetic acid moiety of the organic ligands occupy facial positions of the distorted octahedral coordination polyhedra, whereas the bridging O atom and the N-donors coordinate *trans* with respect to each other.

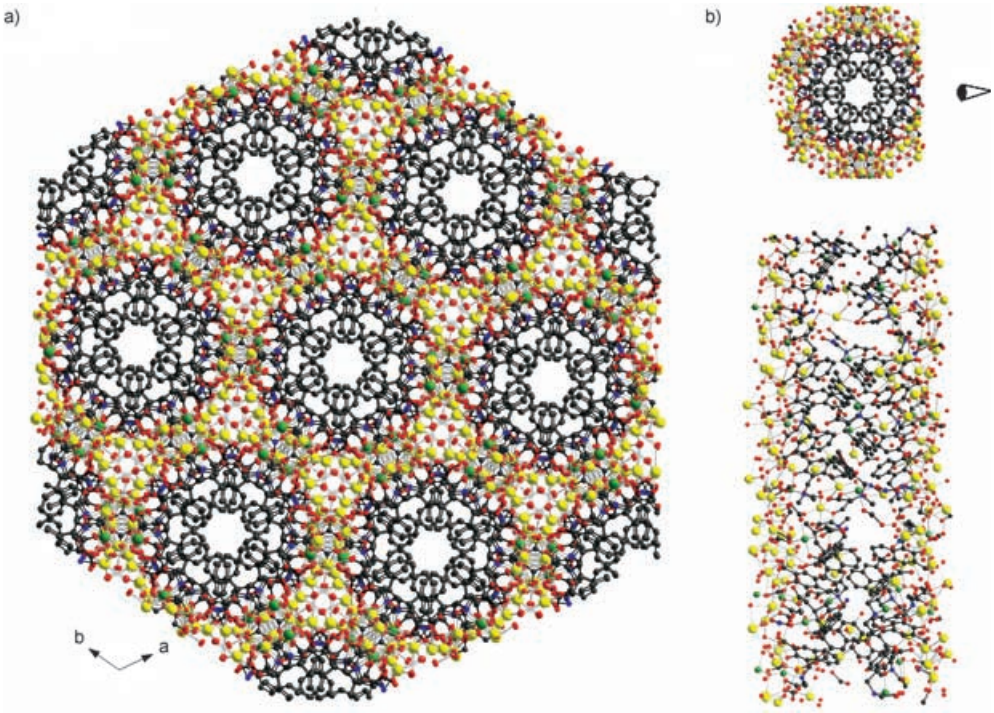

Figure 2. Supramolecular structure of **1**. a) Viewed along the *c* axis. b) Section through a channel viewed perpendicular to the *c* axis. (Fe: green, Na: yellow, O: red, N: blue, C: gray.)

Within the coordination ensemble (Figure 2), the $[Fe_2(\mu\text{-}O)(\mu\text{-}CO_3)(chnida)_2]^{6-}$ complexes are organized in such a way that the organic residues of the ligands are contained in tubular cavities that run along the long axis (crystallographic *c* axis) of the crystals. The intercavity spaces are occupied by hydrated sodium ions which are present to balance the negative charge of the diiron complex and which are linked to the complexes through oxygen donors. The hydrophobic cavities of this honeycomb-type structure have a maximum cross-sectional distance of approximately 1.2 nm. The preponderance for the hexagonal symmetry within the structure is consistent with the morphology of the compound, which crystallizes as needles with a hexagonal cross-section. Single-crystal X-ray analysis of **1** found its structure to be within the trigonal space group $R\bar{3}c$ and demonstrates that **1** is isostructural with its potassium analogue.[11,12] Further confirmation of the space-group assignment was gained from X-ray powder diffraction measurements and simulations (see the Supporting Information). The presence of clearly demarcated nanosized organic and inorganic regions organized into a honeycomb-type structure prompted us to speculate about the synthesis of materials with nanoscale features by using thermal decomposition.

Crystals of **1** are sensitive to solvent loss, and we investigated this behavior by cutting crystals, which had been stored for six weeks at room temperature, perpendicular to the *c* axis by using a focused gallium ion beam. Previously,

we have successfully used electron microscopic techniques to identify structural patterns within crystals[11] and, in this case, the scanning electron microscopy (SEM) observation of the resulting *a*–*b* surface revealed a transformation of some regions of the crystal into fibers with a diameter of approximately 50–100 nm (Figure 3a). These fibers are coagulated into bundles. The IR and UV/VIS spectra and X-ray powder diffraction patterns of the crystals prior to and following desolvation are similar, which demonstrates that the structure of the dinuclear Fe^{III} unit is intact and that the structures of single crystals and the observed hybrid organic–inorganic fibers are closely related.

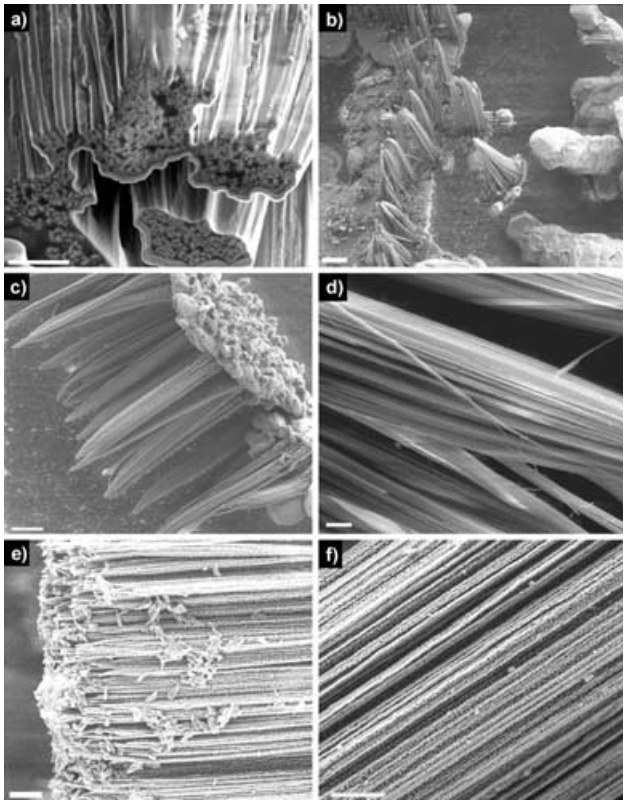

Figure 3. SEM images of **1**: a) A crystal cut perpendicular to the crystallographic *c* axis with a focused ion beam (scale bar: 2 μm). b) Crystals after thermolysis at 370 °C, thus showing fibers and burnt crystals in the same sample (scale bar: 20 μm). c) View of aggregated fibers (scale bar: 20 μm). d) Magnification showing some individual fibers (scale bar: 2 μm). e) and f) Further views of the fibrous structures (scale bars: 2 μm).

Thermolysis of crystals of **1** under nitrogen confirms fiber formation after desolvation (Figure 3b–f) and provides a means for variation of the fiber composition up to their decomposition at approximately 400 °C. Thermogravimetric analysis (TGA), in combination with TGA–MS, IR, and X-ray diffraction (XRD) analysis, provided information about the composition of the sample during thermolysis. On the basis of elemental analysis, the formula $Na_6[Fe_2(\mu\text{-}O)(\mu\text{-}CO_3)(chnida)_2]\cdot 9H_2O$ was assigned to crystalline samples of **1** used in this study. TGA events (Figure 4a) in the temperature range 25–140 °C result from solvent loss. The thermolytic destruction of the Fe^{III} complex occurs during the event between 250 and 350 °C and is accompanied by the formation of sodium carbonate, as demonstrated by FTIR and X-ray powder diffraction analysis (Figure 4b–d).[13] Samples thermolyzed at 350–370 °C were black in appearance because of deposition of amorphous carbon in the sample. This amorphous carbon was detected by TGA-MS (*m*/*z* 12 amu), and its formation is attributed to combustion of the ligand in an anoxygenic environment, such as that in the tubular channels of the crystals. This process is commonplace in the pyrolysis of organic molecules within zeolite templates in which efficient carbonization occurs at elevated temperatures.[14]

The combustion of the remnant carboniferous materials occurs between 380 and 480 °C. During this event, samples contain Na_2CO_3 and iron oxide species which further react between 480 and 600 °C with the loss of dioxide lost from the sample to form $NaFeO_2$.[15] X-ray powder diffraction patterns of samples of **1** heated to 600 °C identify the trigonal and orthorhombic phases of $NaFeO_2$ and γ-Na_2CO_3. Upon heating the sample to 1100 °C, sodium carbonate is no longer present and only the orthorhombic form of the binary sodium iron oxide can be observed (Figure 4c,d).[16]

We analyzed thermolyzed samples using scanning electron microscopy (SEM). Decomposition temperatures were selected by reference to thermogravimetric (TG) and differential thermogravimetric (*d*TG) data. Thus, the plateau between 350 and 390 °C in the *d*TG trace was selected as being of interest as it marks a borderline for the hybrid material transforming into purely inorganic product. At this point, the sample appears to be between two distinct weight losses. From the TGA–MS analysis, the first event entails loss of water, carbon dioxide, and small quantities of both benzene and naphthalene, whereas the second is dominated by loss of carbon monoxide, carbon dioxide, and water, together with benzene and other fragments from the incomplete combustion of the ligand. The SEM micrographs shown in Figures 3b–f and 5b show the result of the thermolysis of **1** at 370 °C and illustrate the formation of a highly aligned fibrous structure.

The energy dispersive X-ray analysis (EDAX) analysis confirms the presence of sodium carbonate in the fibrous material obtained at 370 °C, which is coated with a carbon-rich shell. The fibrous nature of the materials inside a thermolyzed crystal could also be observed through the carboniferous husks at several sites (see also Figure 5b). Closer observation of the fibers reveals that they have a cross-sectional thickness of 50 nm and tend to be segmented. This segmentation differs from the materials obtained at temperatures below 300 °C, in which the fibers are more homogeneous, or even microcrystalline, and contain the intact dinuclear complex.

To illustrate the structure of the product of the thermolysis of **1** at 370 °C, we have presented a scheme in Figure 5. Our observations and analysis rationalize the following thermally induced transformation process of single crystals. Components in a single crystal of **1** aggregate into fibers upon solvent loss. This process is enhanced by the morphology of the crystals and the supramolecular structure of the coordination compound, which contains nanosized channels of

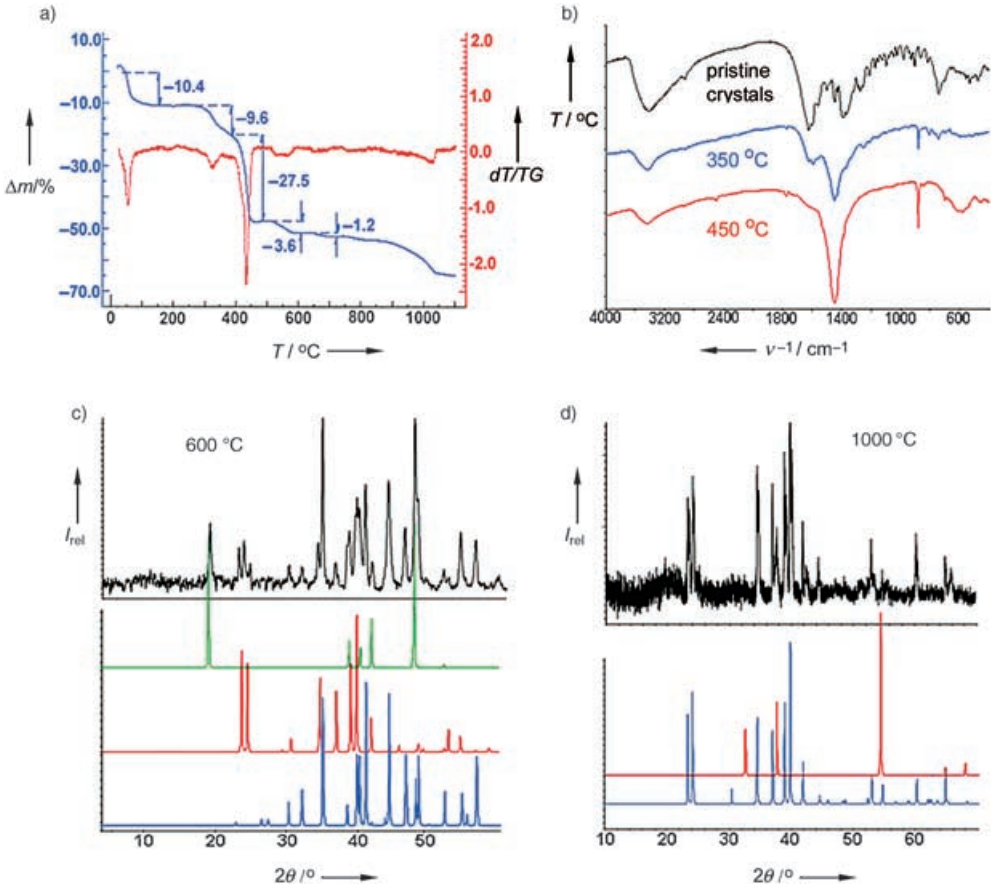

Figure 4. a) Thermogravimetric analysis of **1**. b) FTIR spectra of **1** and thermolyzed samples. c) XRD pattern of **1** thermolyzed to 600 °C; identification of the components was carried out by comparison with generated XRD patterns of trigonal $NaFeO_2$ (green), orthorhombic $NaFeO_2$ (red), and γ-Na_2CO_3. d) XRD pattern of **1** thermolyzed to 1000 °C; comparison with generated XRD patterns of orthorhombic $NaFeO_2$ (blue) and Na_2O (red).

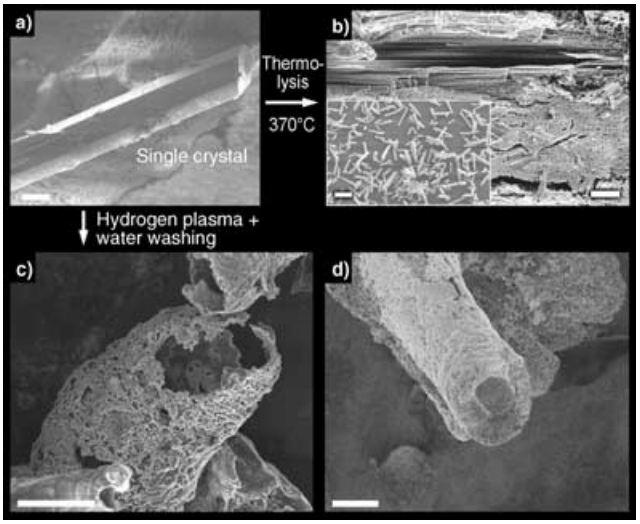

Figure 5. SEM images that illustrate microcapsular formations after crystal decomposition: a) Morphology of a single crystal (scale bar: 10 μm). b) Fibrous structure viewed through a break in the surface of a thermolyzed crystal (scale bar: 2 μm); inset: crystals thermolyzed in bulk (scale bar: 100 μm). c) Carbon microcapsule formed during plasma treatment of crystals of **1** after washing with water (scale bar: 10 μm). d) Cross-sectional view of broken carboniferous microcapsule (scale bar: 5 μm).

clearly separated polarity that run parallel to the longitudinal axis of the needlelike crystals. Heating of the resulting hybrid organic–inorganic fibers to 370 °C causes a chemical transformation in which they form sodium carbonate by decomposition of the dinuclear complex. The facile formation of sodium carbonate upon heating is dictated by the stoichiometry and the structure of the complex, which contains a large number of alkali-metal counterions that bind to carbonate and carboxylate oxygen atoms and are localized in the hydrophilic regions. Naphthoic acid derivatives are known to undergo facile decarboxylation upon heating, and the Na_2CO_3 formation is likely to be the result of this and other decomposition reactions. Further ligand decomposition at 370 °C and at higher temperatures enriches the carbon content at the outside of the burnt crystals so that sodium carbonate fibers are usually contained within capsules composed of amorphous carbon. Thus, it is relatively simple to remove the sodium carbonate by washing with water to leave the empty carbon capsule of micrometer dimensions, which is determined by the morphology of the crystalline precursor. Furthermore, it is possible to improve the formation of amorphous carbon by the application of a reductive process to the crystals of **1**, whereby the crystals are treated with a plasma of hydrogen gas at a temperature slightly higher than the decomposition temperature of 400 °C. In that case, much more robust carbon microcapsules are produced, as shown in Figure 5c,d.

High-surface-area sodium carbonates are used for the removal of SO_x, NO_x, HF, and HCl pollutants from industrial emissions.[17] The high activity of these sodium carbonates makes them the preferred substances for dry-sorbent injection processes; thus, they are used for flue-gas desulfurization and scrubbing, effectively decreasing the impact of acid rain on the environment.[17,18] Therefore, nanostructured particulates, or even better, sodium carbonate nanomaterials contained in microcapsular entities, are of substantial industrial interest. Such alkali or alkali-earth carbonates are currently used as NO_x storage/reduction catalysts for the cleansing of emissions from diesel engines.[19] Furthermore, alkali iron oxide phases also possess high activity for the reduction of

NO_x emissions[20] and are the main active components of the industrially applied Fe_2O_3 dehydrogenation catalyst for the production of styrene from ethylbenzene.[21] It is interesting that we obtain such alkali iron oxides (e.g., the different phases $NaFeO_2$, $KFeO_2$, and $K_xFe_{22}O_{34}$ ($x = 2$–4)) in our system, albeit at elevated temperatures.

In summary, we have demonstrated that a hybrid organic–inorganic coordination complex with an extended 3D structure that contains separated organic and inorganic regions can be used as a template in thermal decomposition reactions that produce nano- and microsized products. Comparable thermolysis studies of crystals of such a hybrid compound have not been reported, and our results validate a synthetic concept for the preparation of nanostructured materials by taking advantage of a pristine crystalline coordination compound that contains the starting components from the thermolysis reaction that are prearranged in a 3D form. Thus, the molecular structure, stoichiometry, and crystal morphology of the precursor determines the 3D structure and constitution of the decomposition products: we obtained aligned nanosized hybrid organic–inorganic fibers by desolvation. Thermolysis changes the fiber composition and results in mainly fibrous sodium carbonate and a concomitant deposition of amorphous carbon at the crystal surface. If sufficient carbon is deposited, stable microcapsules can be obtained after removal of the sodium carbonate by washing with water, thus leaving the carbon microcapsules intact. The components react at higher temperatures to give different phases of sodium iron oxides. We are currently investigating the inorganic products obtained from thermolysis of **1** by transmission electron microscopy (TEM). In addition, we are preparing derivatives of **1** in which sodium ions have been substituted with a variety of metal ions and are carrying out thermolysis of these novel supramolecular transition-metal assemblies under different atmospheres.

Experimental Section

The starting materials were purchased from Aldrich Chemical Co. and used without further purification. Thermogravimetric analyses were carried out using a Netzsch STA 409C operating in the TG mode under both nitrogen and oxygen. TGA–MS measurements were performed on a similar device equipped with a quadrupole mass detector by using electron impact ionization. In that case, the analysis was done under vacuum. Scanning electron micrographs were obtained using a LEO 1530 SEM with a spatial resolution of 1 nm at 20 kV and 3 nm at 1 kV and equipped with an energy-dispersive X-ray analysis system EDX INCA 400 from Oxford Instruments. Focused ion-beam sectioning and scanning-electron micrographs of the sections were obtained using a FEI 200 × P dual beam SEM/FIB. FTIR spectra were obtained with KBr pellets of the analytes with a Perkin-Elmer Spectrum One spectrophotometer. XRD analysis was performed on a STOE Stadi *P* diffractometer (equipped with Ge monochromator) using $Co_{K\alpha}$ radiation ($\lambda = 1.78897$ Å). Sample thermolysis of **1** was performed using a Netzsch STA 409C apparatus with sample heating and cooling rates of 2 or 5 °C min^{-1}. The sample was held isothermally at the selected thermolysis temperature for 1 min.

The chnida ligand was prepared by the Mannich reaction[22] of 3-hydroxy-2-naphthoic acid: ^{1}H NMR ($D_2O + Na_2CO_3$): $\delta = 3.62$ (s, 4H), 4.35 (s, 2H), 7.42 (m, 1H), 7.65 (m, 1H), 7.86 (d, 1H, J(H,H′) = 8.0 Hz), 7.99 (d, 1H, J(H,H′) = 8.6 Hz), 8.29 ppm (s, 1H).

1: Ligand chnida (0.088 g, 2.64×10^{-4} mol) was treated with iron(III) chloride hexahydrate (0.142 g, 5.28×10^{-4} mol) in methanol (30 mL), followed by addition of 2 M aqueous sodium hydroxide (2 mL). Ethanol (20 mL) was added after dissolution of all reagents, and the solution container was covered with parafilm, which was perforated several times to allow slow evaporation of the solvent. It is vital that the solution is open to the atmosphere to allow dissolution of carbon dioxide into the reaction mixture. Small well-formed needles with a hexagonal base of **1** formed after 10 days. Yield: 0.09 g (56% based on chnida). Elemental analysis (%) calcd for ($C_{33}H_{49}Fe_2N_2Na_6O_{31.5}$): C 32.3, H 4.0, N 2.3; found C 32.6, H 4.2 N 2.4.[23]

Received: May 20, 2005
Published online: October 13, 2005

Keywords: iron · nanostructures · organic–inorganic hybrid composites · supramolecular chemistry · thermochemistry

[1] *Encyclopedia of Nanoscience and Nanotechnology, Vol. 1–10* (Ed.: H. S. Nalwa), American Scientific Publishers, CA, **2004**.
[2] a) R. Schlögl, S. B. A. Hamid, *Angew. Chem.* **2004**, *116*, 1656–1667; *Angew. Chem. Int. Ed.* **2004**, *43*, 1628–1637; b) N. Pinna, M. Willinger, K. Weiss, J. Urban, R. Schlögl, *Nano Lett.* **2003**, *3*, 1131–1134.
[3] a) D. A. Doshi, N. K. Huesing, M. Lu, H. Fan, Y. Lu, K. Simmons-Potter, B. G. Potter, A. J. Hurd, C. J. Brinker, *Nature* **2000**, *406*, 107–111; b) *Future Trends in Microelectronics* (Eds.: S. Luryi, J. Xu, A. Zaslavsky), Wiley-VCH, Weinheim, **2004**.
[4] a) M. Brorson, T.W Hansen, C. J. H. Jacobsen, *J. Am. Chem. Soc.* **2002**, *124*, 11582–11583, and references therein; b) J. Ruokalainen, G. ten Brinke, O. Ikkala, *Adv. Mater.* **1999**, *11*, 777–780; c) G. J. de A. A. Soler-Illia, C. Sanchez, B. Lebeau, J. Patarin, *Chem. Rev.* **2002**, *102*, 4093–4138; d) C. N. R. Rao, M. Nath, *Dalton Trans.* **2003**, 1–24.
[5] a) *Handbook of Organic–Inorganic Hybrid Materials and Nanocomposites, Vol. 1* (Ed.: H. S. Nalwa), American Scientific Publishers, CA, **2003**; b) O. M. Yaghi, M. O'Keeffe, N. W. Ockwig, H. K. Chae, M. Eddaoudi, J. Kim, *Nature* **2003**, *423*, 705–714; c) P. M. Forster, A. K. Cheetham, *Angew. Chem.* **2002**, *114*, 475–477; *Angew. Chem. Int. Ed.* **2002**, *41*, 457–459.
[6] C.-Y. Su, A. M. Goforth, M. D. Smith, P. J. Pellechia, *J. Am. Chem. Soc.* **2004**, *126*, 3576–3586.
[7] K. Knoth, R. Hühne, S. Oswald, L. Schultz, B. Holzapfel, *Supercond. Sci. Technol.* **2005**, *18*, 334–339.
[8] For example: a) J. Xu, M. Ekblad, S. Nishiyama, S. Tsuruya, M. Masai, *J. Chem. Soc. Faraday Trans.* **1998**, *94*, 473–479; b) T. Mishra, K. Parida, *J. Mater. Chem.* **1997**, *7*, 147–152.
[9] a) G. Ozin, *Chem. Commun.* **2000**, 419–432; b) M. Eddaoudi, J. Kim, N. Rosi, D. Vodak, J. Wachter, M. O'Keeffe, O. M. Yaghi, *Science* **2002**, *295*, 469–472; c) N. L. Rosi, J. Eckert, M. Eddaoudi, D. T. Vodak, J. Kim, M. O'Keeffe, O. M. Yaghi, *Science* **2003**, *300*, 1127–1129; d) G. Férey, M. Latroche, C. Serre, F. Millange, T. Loiseau, A. Percheron-Guégan, *Chem. Commun.* **2003**, 2976–2977.
[10] W. Schmitt, M. Murugesu, J. C. Goodwin, J. P. Hill, A. Mandel, R. Bhalla, C. E. Anson, S. L. Heath, A. K. Powell, *Polyhedron* **2001**, *20*, 1687–1697.
[11] a) W. Schmitt, J. P. Hill, M. P. Juanico, A. Caneschi, F. Costantino, C. E. Anson, A. K. Powell, *Angew. Chem.* **2005**, *117*, 4259–4264; *Angew. Chem. Int. Ed.*, **2005**, *44*, 4187–4192; b) W. Schmitt, C. E. Anson, J. P. Hill, A. K. Powell, *J. Am. Chem. Soc.* **2003**, *125*, 11142–11143.
[12] Cell dimensions of **1**: space group $R\bar{3}c$, $a = 35.301(4)$, $c = 43.356(6)$ Å, $V = 46719(9)$ Å^3, $Z = 36$; for isostructural potassium compound[11] $K_6[Fe_2(\mu\text{-}O)(\mu\text{-}CO_3)(chnida)_2]\cdot 13.5\,H_2O$

(CCDC-262831): $C_{33}H_{49}Fe_2K_6N_2O_{31.5}$, $R\bar{3}c$, $a = 35.3692(10)$, $c = 43.3010(18)$ Å, $V = 46911(3)$ Å^3, $Z = 36$. The high-quality structural refinement of **1** was impossible as the single crystals diffracted weakly and no dataset with a satisfactory I/σ ratio was successfully obtained; however, single-crystal X-ray analysis confirms the identity of the compound. Powder diffraction patterns of **1** and generated patterns (generated on the basis of the structure given in Figure 2 and the coordinates of the isostructural K^+ analogue) agree well (see the Supporting Information). Microanalytical data for freshly-prepared crystals of **1** were also in good agreement with the formulation $Na_6[Fe_2(\mu\text{-}O)(\mu\text{-}CO_3)(chnida)_2]\cdot 13.5\,H_2O$ analogous to the K^+ compound (see the Experimental Section).

[13] IR data: A. K. Shokanov, M. I. Bakeev, *Akad. Nauk Kaz. SSR* **1967**, *3*, 102; powder XRD data: W. v. Aalst, J. den Holander, W. J. A. M. Peterse, P. M. de Wolff, *Acta Crystallogr. Sect. B* **1976**, *32*, 47–58; comparison of the IR spectra reveals that parts of the organic ligand are still intact at 350 °C but that symmetric and antisymmetric stretching vibrations of the carboxylate group (1621 and 1395 cm^{-1}, respectively) are strongly diminished with a concurrent increase in the intensity of the band at 1447 cm^{-1} (symmetric stretching vibration of the carbonate anion) as well as the band at 880 cm^{-1} (antisymmetric deformation of CO_3^{2-}). Loss of complexity in the IR fingerprint region signifies the destruction of the ligand.

[14] a) K. Matsuoka, Y. Yamagishi, T. Yamazaki, N. Setoyama, A. Tomita, T. Kyotani, *Carbon* **2005**, *43*, 855–894; b) Z. Ma, T. Kyotani, A. Tomita, *Chem. Commun.* **2000**, 2365–2366.

[15] The synthesis of $NaFeO_2$ from Na_2CO_3 and Fe_2O_3 is well documented as it is currently being used as an active cathode material in nonaqueous electrolyte batteries: M. C. Blesa, E. Moran, C. León, J. Santamaria, J. D. Tornero, N. Menéndez, *Solid State Ionics* **1999**, *126*, 81–87, and references therein; Y. Takeda, J. Akagi, A. Edagawa, M. Inagaki, S. Naka, *Mater. Res. Bull.* **1980**, *15*, 1167–1172; batteries assembled using $NaFeO_2$ as the cathode material have high discharge capacities and long cycle lives.

[16] Sodium oxide, which must be present, could not be observed in our samples presumably because it is present in a glassy state and transparent to X-ray radiation.

[17] *Ullmann's Encyclopedia of Industrial Chemistry* (Ed.: B. Elvers, S. Hawkins), 7th ed., Wiley-VCH, Weinheim, **2004**.

[18] a) U.S. EPA/DOE/EPRI Combined Power Plant Air Pollutant Control Symposium: *The Mega Symposium*, Proceedings, August 20–23, **2001**, Chicago, Illinois, USA; b) R. Bell, US Patent 19924982672, **1992**; c) *Full-Scale Evaluation of a Multi-Pollutant Reduction Technology: SO_2, Hg, and NO_x*, E. Haddad, J. Ralston, S. Castagnero, Mobotec USA, Inc. **2003**, p. 101; d) *Solvay T-200 Use in Dry Sodium Injection for SO_2 Removal* (Ed.: L. Ninane), Central Study and Research Center, Solvay S.A., Dombasle, France, **1993**.

[19] A. F. Cheffey, P. R. Philips, US Patent, 200500116164, **2005**.

[20] S. Kureti, W. Weisweiler, K. Hizbullah, *Appl. Catal. B* **2003**, 43, 281–291.

[21] P. G. Menon, B. Delmon in *Handbook of Heterogeneous Catalysis, Vol. 1* (Eds.: G. Ertl, H. Knözinger, J. Weitkamp), VCH, Weinheim, **1997**, p. 101.

[22] V. Temkina, M. N. Rusina, G. F. Yaroschenko, M. Z. Branzburg, L. M. Timakova, N. M. Dyatlova, *Zh. Obshch. Khim.* **1975**, *45*, 1564–1570.

[23] Details of the thermogravimetric analysis, the XRD pattern of **1**, and the pattern generated on the basis of the structural model given in Figure 2; XRD, IR, and TGA–MS analysis; and further SEM images of samples thermolyzed at 510 °C and of hybrid organic–inorganic fibers in samples obtained at 250 °C are given in the Supporting Information.

